21

Numerical Modelling for Thermal Design of Electronic Equipments

Giuseppe Petrone and Giuliano Cammarata
Department of Industrial and Mechanical Engineering, University of Catania
Italy

1. Introduction

During the last decades, reproducing physics of systems by computer simulation has aroused great interest both in academic community and industrial world. Disposing of a virtual model, able to simulate the real behaviour of a system, represents a really powerful tool both for understanding phenomenological aspects of a chosen physics and for predicting functional or operative conditions of a technological system. Because of this, large efforts are continuously spent in developing computational codes for specific applications and in building up simulating models in a very wide range of technological domains. Despite of its unquestionable advantages, experimental approach in studying systems often results expensive and hardly flexible. Instead, developing of reliable software, combined with increasing in hardware capability, are more and more encouraging researchers to adopt the simulating approach also in solving complex systems. This opportunity obviously promises wide gaps of optimisation in manufacturing also, with consequent growth in effectiveness and in economic benefit.

Focalising attention on electronic equipments, it is commonly recognized that careful thermal design represents an unavoidable step in pre-production phase (Harvest et al., 2007), in order to ensure reliability and performance of those components during their functioning (Hanreich et al., 2000). Electronic devices produce a very important rate of specific heat (related to their small dimensions) as a by-product of their normal operation. Exceeding in maximum safe operating temperature specified by the manufacturer means a strong reduction of semiconductors efficiency and functional life (Bailey et al., 2002). Among the high power components, Random Access Memory modules are one of the more sensitive thermal subsystem of an assembled computer (Petrone et al., 2007). Cooling of those devices is always performed by mechanical ventilation systems, that assure a forced convection mechanism in order to dissipate thermal energy. However, the forced air flow is often disturbed by many factors. Cables, drive bays and brackets can determinate bypass over the memory components, forcing the subsystem to operate in mixed or natural convection conditions (El Alami et al., 2005). Therefore, natural convection represents a critical heat transfer mechanism assuring cooling if designed operational conditions, for any reason, partially or totally fall down (Bhowmik & Tou, 2005). Otherwise, the passive character of cooling by natural convection makes it very attractive for possible application in electronic devices (da Silva et al., 2005). From a theoretical point of view, cooling of

electronic packages has furthermore created emphasis on understanding the basic convective fluid flow over discrete heat sources (Bae & Hyun, 2004; Dogan et al., 2006), which have different characteristics from the traditionally studied convection from a heated whole wall. This chapter deals with a numerical analysis on natural and mixed convection heat transfer for Dual In-line Memory Modules, both horizontally and vertically disposed. The physical system is firstly introduced, then implementation and validation of the applied numerical model is discussed and finally the main obtained results are illustrated.

2. The physical system

The actually most used Random Access Memories in Personal Computers are the Dual-Inline-Memory-Modules (DIMM). They are made of 4-16 chip of synchrony dynamical memory with random access (SDRAM), type DDR (Double Data Rate) or DDR2. Chips are characterized by very small dimensions and they are mounted on a Printed Circuit Board (PCB). The PCB disposes of a certain number of PIN both on its top and bottom face. An example of a DIMM is reported in Figure 1.

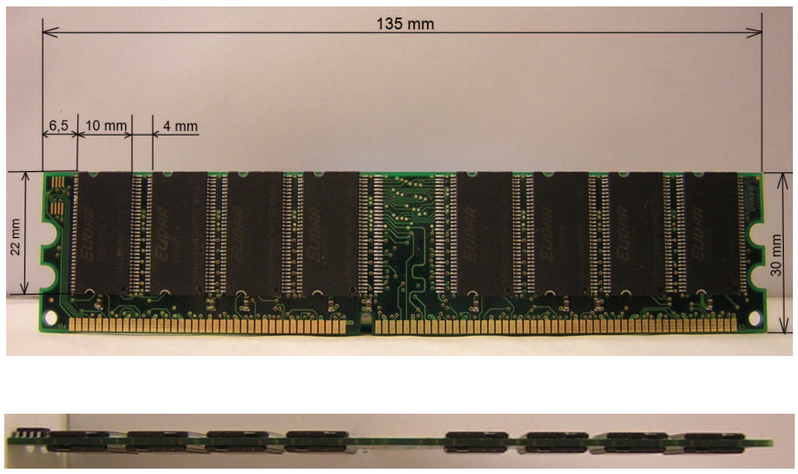

Figure 1. Bottom and backside views of a Dual In-line Memory Module

These components are object of the Joint Electron Device Engineering Council (JEDEC) standards. According to JEDEC specifications, the mean parameter indicating thermal performance of DIMM is the total thermal resistance θ_{TOT} between miniaturized integrated circuit and surrounding environment. This represents the sum of sequential thermal resistances, such as junction-package resistance, package-heat sink resistance (if a heat sink is present), heat sink-ambient resistance (Figure 2). By knowing θ_{TOT} value, it is possible, for a chosen ambient temperature T_{AMB} and for a standard active power of 1 [W], analytically evaluating the junction temperature $T_{JUNCTION}$ of the chip. In order to guarantee the reliability of the memory modules, it is strictly necessary that chip does not overcome, during its functioning, the maximum temperature recommended in the technical documentations of constructors. These values are commonly comprised in the range 80-110 [°C]. Considering a generic vertically disposed mainboard (tower configuration for a PC case), DIMM modules are arranged in horizontal disposition, as showed in the top portion of Figure 3. The PCB, where chips are arranged, is perpendicularly connected to the vertical mainboard by specific sockets with lateral guides.

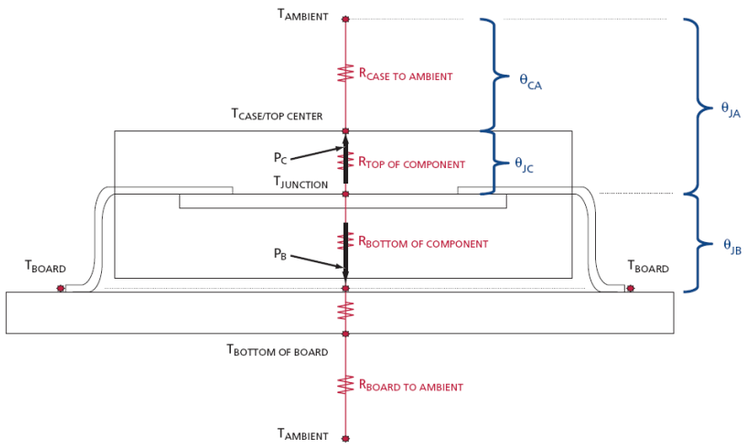

Figure 2. Scheme of a cross section of a chip mounted on a circuit board: primary thermal resistances

For predictive estimation of operative temperature of DIMM, leading constructors recommend computational modelling in spite of analytical determination of temperature by JEDEC indications. In fact analytical determination of $T_{JUNCTION}$ could be not exhaustive because of the lack of consideration of several significant factors, first of all the proximity of other heat sources.

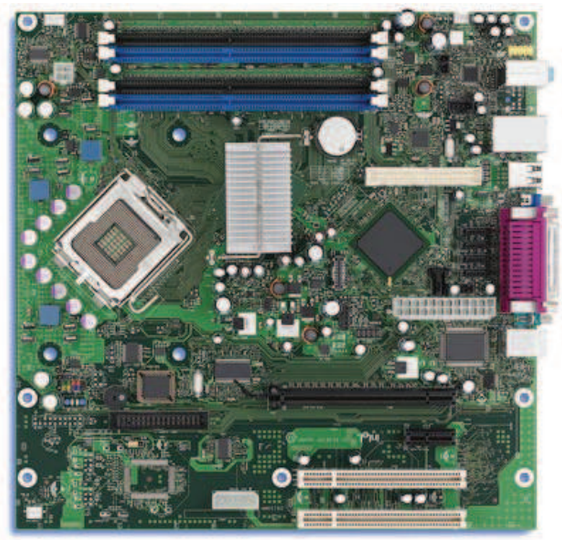

Figure 3. Electronic components arranged on a mainboard of a tower configuration PC

3. The numerical model

3.1 Continuous governing equations

The considered physical system is outlined by parallel boards (Printed Circuit Board) surrounded by air and arranging on multiple heat sources (Chip), see Figure 4.

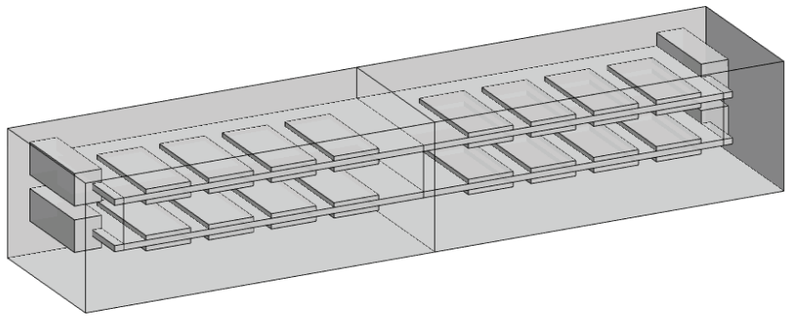

Figure 4. Geometry of two overlapped 16-chip memory modules horizontally arranged

In natural convection, fluid is propelled by the buoyancy force, generated by a non-uniform density distribution due to local temperature gradients. In our problem, heating of fluid is related to the presence of heat sources (chips in operative conditions) plunged in the air volume. The multi-physical problem is mathematically governed by conservation laws, the Navier-Stokes equations, characterizing flow of an incompressible fluid, and the energy equation, defining the equilibrium between heat fluxes (conductive one and convective one) and heat sources. The governing partial differential equations are reported in following:

$$\begin{cases} \rho \dfrac{\partial \vec{U}}{\partial t} + \vec{\nabla} \cdot (\rho \vec{U} \times \vec{U}) = -\vec{\nabla} p + \vec{\nabla}^2 (\eta \vec{U}) + (\rho_0 - \rho)\vec{g} \\ \dfrac{\partial \rho}{\partial t} + \vec{\nabla} \cdot (\rho \vec{U}) = 0 \\ \rho C_p \dfrac{\partial T}{\partial t} + \vec{\nabla} \cdot (\rho C_p \vec{U} T) = q + \vec{\nabla}^2 (kT) \end{cases} \tag{1}$$

The energy equation is to be solved in fluid as well as in solid sub-domains of system, by considering appropriate values for thermal conductivity ($k_C = 163\ [Wm^{-1}K^{-1}], k_p = 0.3\ [Wm^{-1}K^{-1}]$). Only in chip sub-domains the heat source term is different from zero and its value is $q = Q_D \big/ (n_c \Omega_c)$. Adopted properties and conditions for fluid in this study are reported in Table 1.

Parameter	Unit
$M = 0.0288$	$[kg\ mol^{-1}]$
$\mathrm{R} = 8.134$	$[J\ mole^{-1}kg^{-1}]$
$p_a = 101325$	$[Pa]$
$\rho \equiv p_0 M/(RT)$	$[kg\ m^{-3}]$
$\eta \equiv 6,0 \cdot 10^{-6} + 4,0 \cdot 10^{-8} T$	$[Pa\ s]$
$k \equiv \exp(-3,723 + 0,865 \log T)$	$[W\ m^{-1}K^{-1}]$
$C_P = 1100$	$[J\ kg^{-1}K^{-1}]$

Table 1. Dynamical and thermal properties of air

Because of the particular technological interest of this kind of study, it seemed favourable solving conservation equations in their original dimensional form. This item allows to focus attention on the specific electronic device considered and make results directly exploitable by operators in this sector. Otherwise, classical non dimensional groups are also used in post-processing of results. The Reynolds number, defined as $\mathrm{Re} \equiv \rho U D_h / \eta$, is evaluated basing on the hydraulic diameter of the inlet section for air flow (lateral or bottom face according to vertical or horizontal arrangement), while the characteristic linear dimension adopted for Rayleigh number evaluation ($Ra \equiv g h^3 \Delta\rho / (\eta\alpha)$) is the distance h between the overlapped circuit boards.

3.2 Solving procedure

Continuous conservation equations (1) are discretized by Finite Element Method (FEM) on no-structured computational meshes, made of tetrahedral elements. The totality of simulations presented in this study have been carried-out by applying the software Comsol Multiphysics®. Discrete equations are solved with boundary conditions defined below:
Fluid-dynamical conditions:

- No-slip conditions on interfaces between fluid and solid elements;
- Constant pressure values on horizontal boundaries of the fluid domain (inlet velocity for mixed convection models);
- Symmetry conditions on lateral end-section of the fluid domain (simplified models only);

Thermal conditions:

- Adiabatic condition for external walls of circuit boards and socket;
- Convective heat flux for top and lateral boundaries of the fluid domain;
- Imposed temperature for the bottom boundary of the fluid domain;

Time-integration of equations (1) has been only performed in order to compare numerical results with experiments (validation of the numerical model), to compare results of transient analysis with steady solution of conservation equations (validation of the steady approach in solving governing equations), to investigate on transient fluid-dynamics during heating of fluid at initial rest conditions. The temporal integration lies on a backward Euler method and the solver is an implicit time-stepping scheme solving a nonlinear system of equations at each time step (Brenan et al., 1989). In order to simplify the presentation of the adopted algorithm for steady solution of equations (1), let now indicate as $\vec{S} \equiv (\vec{U}, T)^t$ a generic solution of Navier-Stokes and energy equations, and let consider the following assumptions for grouping transport, diffusion, buoyancy and pressure terms (Petrone et al., 2004):

$$[\mathcal{T}(\vec{U})](\vec{S}) = -\begin{pmatrix} \vec{\nabla}\cdot(\rho\vec{U}\times\vec{U}) \\ \vec{\nabla}\cdot(\rho C_p \vec{U} T) \end{pmatrix}$$

$$\mathcal{D}(\vec{S}) = \begin{pmatrix} \vec{\nabla}^2(\eta\vec{U}) \\ \vec{\nabla}^2(kT) \end{pmatrix}$$

$$\mathcal{B}(\vec{S}) = \begin{pmatrix} (\rho_0 - \rho)\vec{g} \\ 0 \end{pmatrix}$$

$$[\mathcal{P}(\vec{U})](\vec{S}) = -\begin{pmatrix} \vec{\nabla} p \\ 0 \end{pmatrix}$$

If $\vec{S}_0 \equiv (\vec{U}_0, T_0)^t$ is a steady solution of equations (1) then it verifies the following expression:

$$[\mathcal{T}(\vec{U}_0) + \mathcal{D} + \mathcal{B} + \mathcal{P}(\vec{U}_0)](\vec{S}_0) = \vec{0} \tag{2}$$

An iterative approximation of steady state $\vec{S}_0$ by $\vec{S}^{(k+1)}$ is performed by applying a modified Newton-Raphson method (Deuflhard, 1974), where a damping factor $0 < \lambda \leq 1$ is introduced in computing of perturbation, as in following:

$$\begin{cases} J_{\mathcal{T}(\vec{U})+\mathcal{D}+\mathcal{B}+\mathcal{P}(\vec{U})}[\vec{S}^{(k)}](\overrightarrow{\delta S}^{(k+1)}) = \\ -[\mathcal{T}(\vec{U}^{(k)}) + \mathcal{D} + \mathcal{B} + \mathcal{P}(\vec{U}^{(k)})](\vec{S}^{(k)}) \\ \vec{S}^{(k+1)} = \vec{S}^{(k)} + \lambda \overrightarrow{\delta S}^{(k)} \end{cases} \tag{3}$$

where the Jacobian operator $J_{\mathcal{T}(\vec{U})+\mathcal{D}+\mathcal{B}+\mathcal{P}(\vec{U})}$, expressed in $\vec{S}^{(k)}$ and applied to perturbation $\overrightarrow{\delta S}^{(k+1)}$, consists in difference between perturbed and not perturbed conservation equations linearized close to the $\vec{S}^{(k)}$ state.

Once $\vec{S}^{(k+1)}$ evaluated, the relative error $E^{(k+1)}$ is computed :

$$J_{\mathcal{T}(\vec{U})+\mathcal{D}+\mathcal{B}+\mathcal{P}(\vec{U})}(\vec{S}^{(k)})E^{(k+1)} = -[\mathcal{T}(\vec{U}^{(k+1)}) + \mathcal{D} + \mathcal{B} + \mathcal{P}(\vec{U}^{(k+1)})](\vec{S}^{(k+1)}) \tag{4}$$

If $E^{(k+1)} > E^{(k)}$ then the code reduces the damping factor λ and computes $\vec{S}^{(k+1)}$ again. This algorithm repeats the damping-factor reduction until the relative error is less than in the previous iteration or until the damping factor underflows the imposed minimum value. When it has taken a successful step $\vec{S}^{(k+1)}$, the algorithm proceeds with the next Newton iteration. A value of $\lambda = 1$ results in classical Newton's method, which converges at second order if the initial guess is sufficiently close to the solution. The iterative procedure ends when:

$$\varepsilon = \left(\frac{1}{N} \sum_{i=1}^{N} \left(\frac{\left| E_i^{(k+1)} \right|}{\left| S_i^{(k+1)} \right|} \right)^2 \right)^{1/2} < \varepsilon_0$$

where N is the number of degrees of freedom for the system and ε_0, fixed at value 10^{-6} in this study, is an arbitrary small number. Algebraic systems coming from differential operators

discretisation are solved by using a direct unsymmetrical multi-frontal method, particularly indicated in order to solve sparse matrix by LU decomposition. Computations have been carried-out on a 64 bit workstation of 16 GB of RAM.

3.3 Computational grid studying

Influence of computational grid has been preliminary studied in order to assure mesh-independent results. The numerical approach in solving continuous equations consists in fact in researching an approximate solution of the exact one. The effectiveness of this approximation primary depends by the degree of spatial discretisation for differential operators. In Table 2 we report a summary of the mesh studying obtained for the horizontal configuration of the DIMM. Relative gaps of maximum of temperature and velocity values over all the domains with respect to reference ones (evaluated for the finest tested grid) indicate that a mesh made of 24611 nodes (139857 degrees of freedom, d. o. f.) can be adopted assuring very small sensitivity of results with spatial discretisation. Saturation of error with increasing in mesh refinement is otherwise well testified by Figure 5, where maximum of velocity is reported as function of the number of elements of the computational grid. Further increasing in mesh refinement does not correspond to substantial benefit in precision justifying much more higher computational time.

Elements	Increasing (%)	d. o. f.	T_{max} [°C]	Relative gap (%)	U_{max} [m/s]	Relative gap (%)
7052	-	38791	85.61	2.60	0.159	13.14
9871	40.0	55108	86.24	1.87	0.153	9.08
14128	43.1	79140	87.13	0.86	0.147	4.85
24611	74.2	139857	87.74	0.17	0.142	1.34
39536	60.6	225600	87.89	-	0.140	-

Table 2. Maximum values of temperature and velocity as function of the number of mesh elements and relative degrees of freedom. Relative gap with respect to reference values (values obtained for the finest grid) are also reported

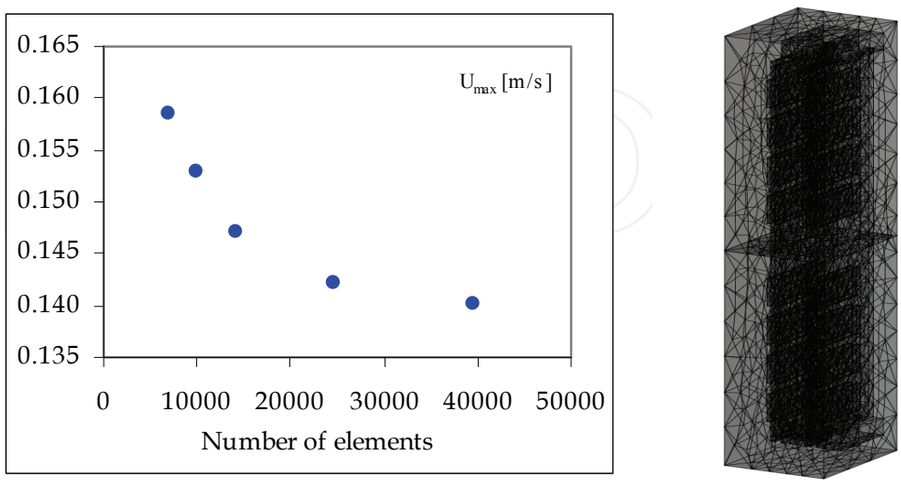

Figure 5. Maximum velocity values reported as function of the elements number for the computational grid (left side) and example of computational grid (right side)

4. Validation of the numerical model

One of the great problem related to the numerical approach in solving the governing equations of a physical system concerns reliability of the adopted simulating model and consequently reliability of the results carried-out by applying the chosen scheme (Towashiraporn, 2004). For that reason it is always advisable firstly testing its reliability. One suitable way to proceed consists in comparing results carried-out by applying the proposed scheme with data concerning similar systems proposed by other researchers and at disposal in scientific literature. Otherwise, sometime this way to proceed could be not possible because we do not dispose of all information needed for exactly replying physical systems studied by other researchers or we are approaching a new problem whose no results are present in literature. The second way to operate (probably better than the previous one) consists, when possible, in setting-up an experimental apparatus reproducing a test section of the physical system we are interested to investigate. By conducing test experiments on this set-up, some data become available to be compared with those obtained by using the numerical model to solve the same configuration of the system. This procedure assures the opportunity of disposing of all technical information needed to reproduce by a virtual model the real system we are studying. Once the numerical model validated by comparison with experimental data, it can be applied to investigate some other configurations (arrangement of components, geometrical dimensions, load conditions, boundary conditions, influence of specific parameters), exploiting all the facilities offered by disposing of a reliable virtual model simulating a real system.

4.1 Comparison with literature results

An example of the first above discussed procedure to validate the numerical model is discussed in this subparagraph. Results of simulation for vertical channels with multiple heat sources plunged in air, have been compared with those experimentally obtained in literature (Ortega, 2002). In Figure 6 we report geometry, thermal and fluid-dynamical fields obtained by numerical models built in conformity with respect to the system analysed in the reference.

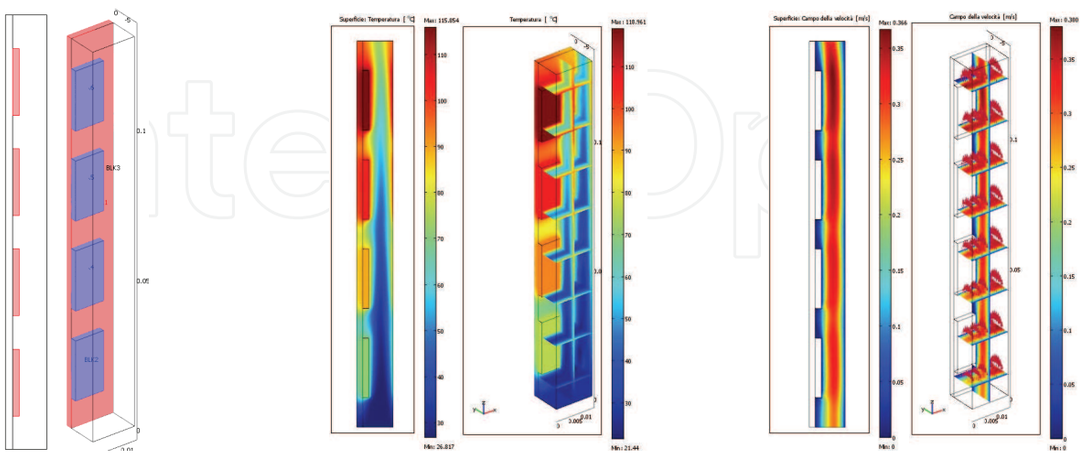

Figure 6. Geometry, thermal fields and velocity fields of the numerical model built for validation with experimental results previously published (Ortega, 2002)

In Figure 7 thermal transmittance K_{0i} between the i-heat source surface (4 surfaces for the presented model) and inlet section for fluid, obtained both for 2D and 3D numerical models, are compared with experimental results of the reference. The compared thermal transmittance is defined as:

$$K_{Oi} = \frac{\frac{1}{\Sigma_1}\int q_i d\Sigma_1}{\frac{1}{\Sigma_2}\int T_{s,i} d\Sigma_2 - T_{f,0}}$$

where Σ_1 and Σ_2 are the total and vertical surface of the heat sources respectively, q_i is the specific thermal flux and $T_{f,0}$ and $T_{s,i}$ are the inlet temperature for fluid and the i-vertical surface mean temperature respectively.

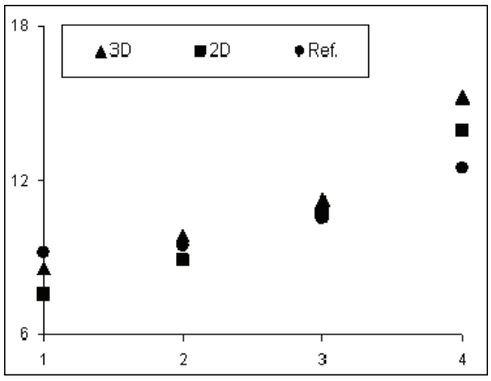

Figure 7. Comparison of thermal transmittance [W/(m²K)] for vertical channels in natural convection conditions between present 2D (square) and 3D (triangle) numerical results and those reported in the reference (circle)

From Figure 7 a good agreement between present results and those published in the reference is evident. Remarkable small gaps between present results with respect to reference could be due to thin difference in geometrical dimension of systems.

4.2 Comparison with experiments

During this study an experimental set-up was also used in order to validate reliability of the adopted numerical procedure for solving thermal and fluid-dynamical fields of the studied system. The experimental technique chosen to produce comparing data for numerical results lies on a thermo-graphic investigation on surfaces thermal distribution of Dual In-line Memory Modules during operative conditions. The experimental apparatus mainly consists in a test PC where two 16-chip memory modules (DDR - 512 MB - 266 MHz) were arranged on, an infrared camera (ThermaCAM Flir SC 3000) for detection of surface thermal fields and a laptop PC used for acquisition (Figure 8). In order to reproduce the most critical heat transfer condition of functioning for the electronic devices, some black panels were employed in order to shield the memory modules by the forced air-flow produced by ventilators. The black box built around the investigated devices also resulted helpful for thermo-graphical acquisition. In fact other hot electronic components mounted on the mainboard were hindered by the black panels, allowing to set temperature range of

the acquisition system with thermal values characteristic of the memory modules we were interested to record. During experimental running specific applications were launched on the test PC in order to load memories by a known electrical power (0.3-0.4 [W]).

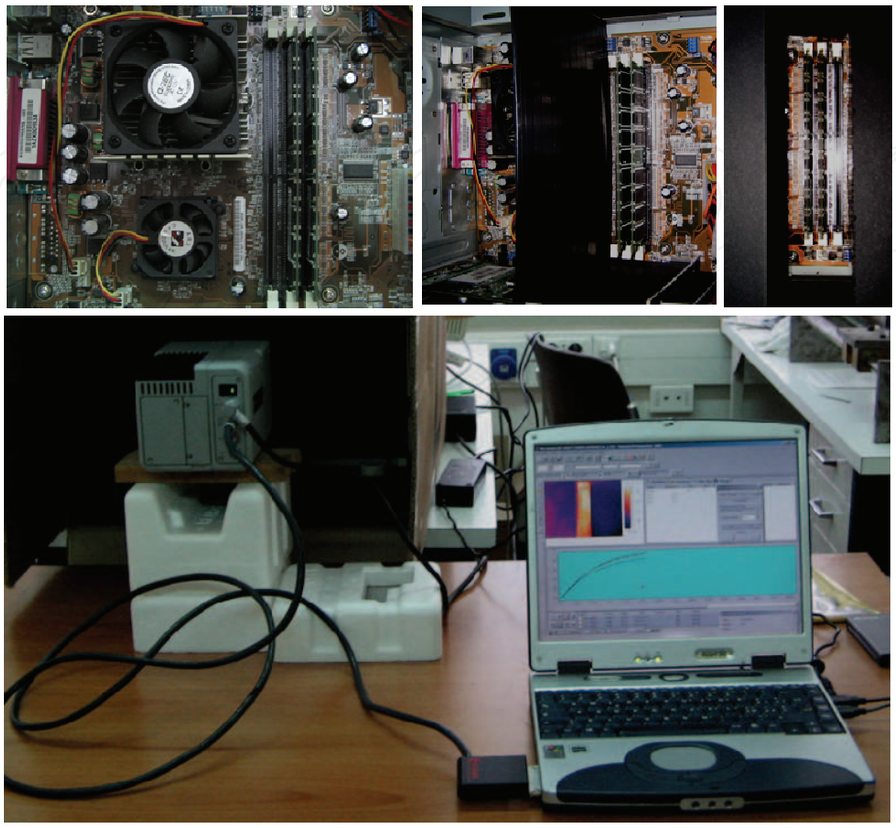

Figure 8. Experimental set-up for thermo-graphic acquisition of thermal levels on DIMM surfaces during functioning under controlled load conditions

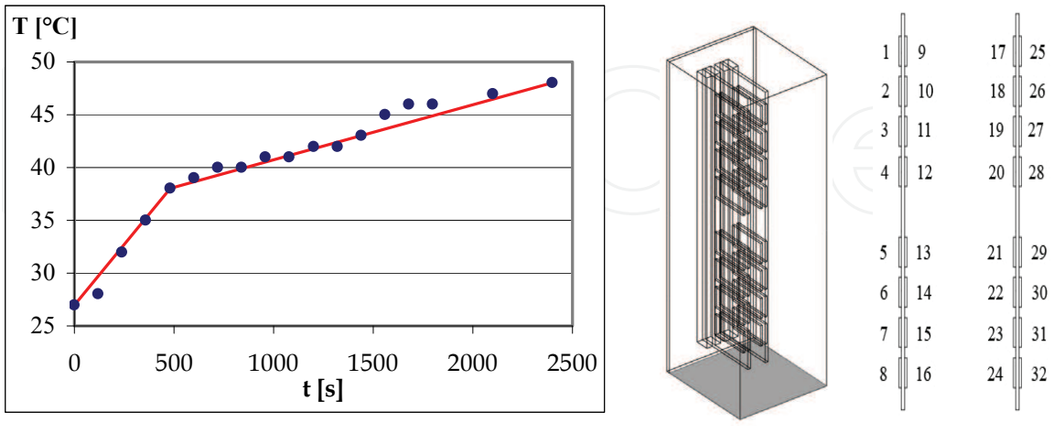

Figure 9. Time-evolution of air temperature experimentally detected at the bottom end of the DIMM (blue dots) and linear functions (red lines) used for implementing the bottom face boundary condition of the numerical model (grey surface). Adopted numeration of the Integrated Circuit for the studies devices (right side of the figure)

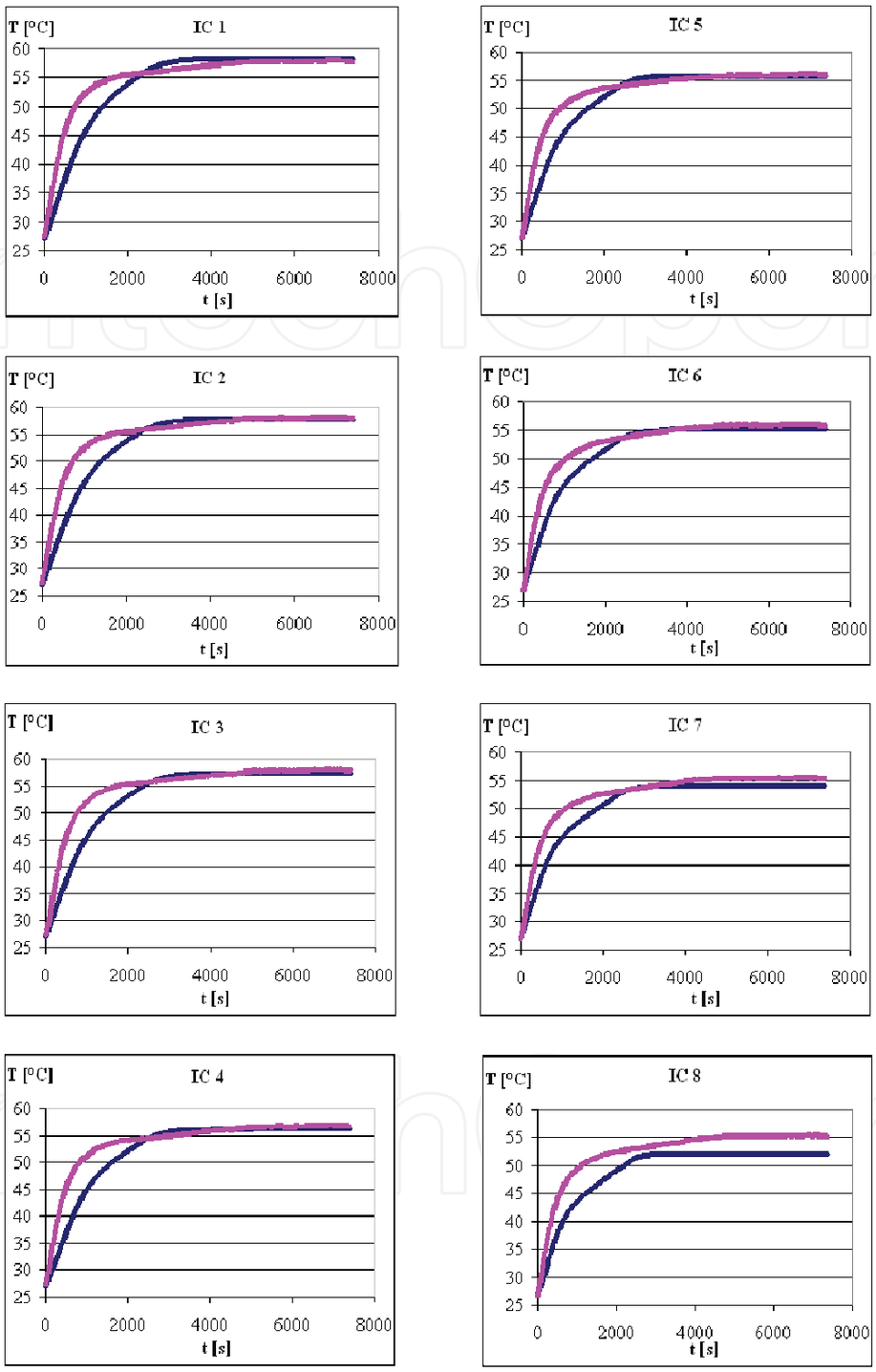

Figure 10. Time evolution of temperature values detected on experimental (pink line) and numerical (blue line) frontal surfaces of the chip (IC 1-8 according to numeration of Figure 9)

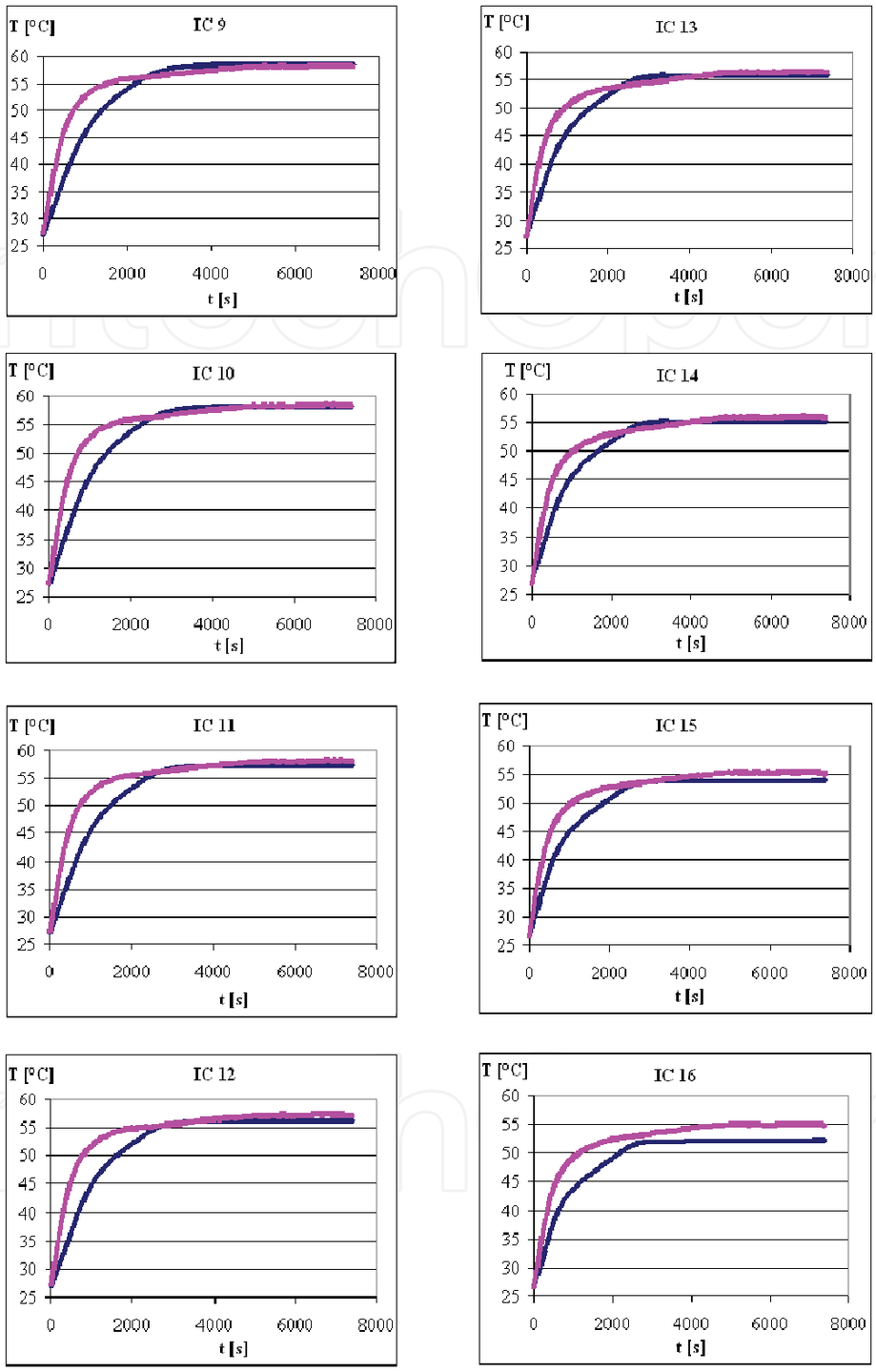

Figure 11. Time evolution of temperature values detected on experimental (pink line) and numerical (blue line) frontal surfaces of the chip (IC 9-16 according to numeration of Figure 9)

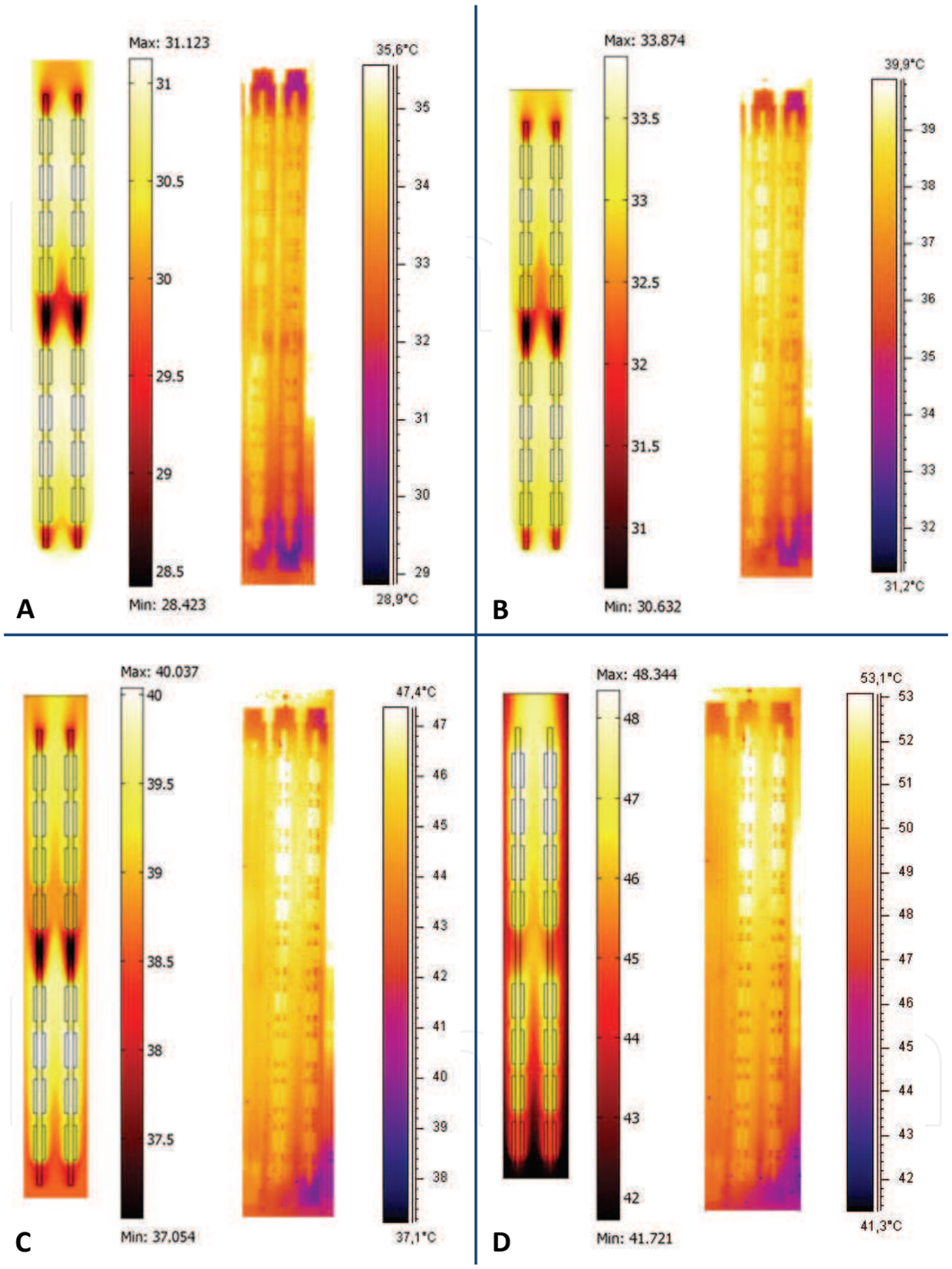

Figure 12. Comparison between numerical and experimental thermal distribution at time steps t=180 (A), t=300 (B), t=600 (C), t=1200 (D)

The experimental acquisitions were recorded each 5 seconds, both for vertical and horizontal arrangement of the case, during a transient time of 3-4 hours. Exceeded this time a stationary thermal behaviour was reached by the dissipating components. Once the test

section built-up under the laboratory facility, numerical models were implemented exactly corresponding to geometrical dimensions and applied thermal load of the test section. Then numerical simulations were carried-out both in transient and in steady conditions for comparing results with the experimental ones. In running transient simulations, the imposed temperature value at the bottom boundary of the air volume surrounding the memory modules (T_{AMB}) was assigned as a time-dependent function, approximating, by two linear functions, the temporal evolution of temperature, experimentally detected by a thermometer arranged at the bottom of the slots of the test set-up (Figure 9), in the time-range 0-2400 [s]. Then it was considered constant. Numerical results were then compared with experimental data obtained by the infrared thermo-graphical investigation. In Figure 10 and Figure 11 time evolution of the mean temperature values detected on 16 experimental and numerical frontal surfaces of the chip arranged on one of the two memory modules are reported. From comparison a very good agreement in transient evolution is clearly observable. Special attention was paid to investigate on comparison between experimental and numerical thermal fields in the time range during which the wider difference was pointed-out. In Figure 12 we report thermal fields obtained by experimental (on the right side) and numerical (on the left side) analysis at time steps t=180 (A), t=300 (B), t=600 (C), t=1200 (D). It is to notice that pictures presented in Figure 12 underline the most unfavourable detected conditions in comparing results coming from experimental and numerical investigation. The experimental thermal values are generally higher than the numerical ones during the initial portion of the transitory. This item could be explained by considering that during PC starting-up several other electronic components, very close arranged to memory modules, dissipate an high rate of thermal energy. This heating contribution is not considered in the numerical model, so that it underestimates thermal level of the memory modules during the first range of the transitory. Otherwise, Figure 13 shows distribution of the mean temperature computed on each chip frontal surface once achieved a thermal steady state.

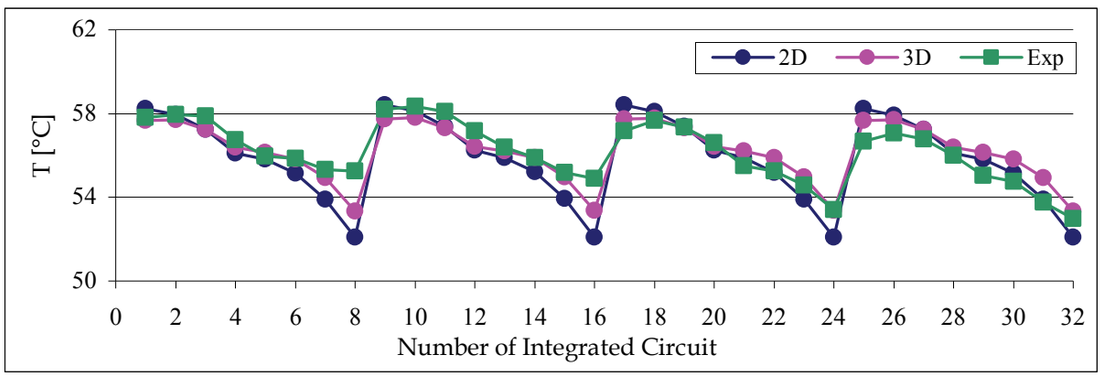

Figure 13. Comparison between steady mean temperature on each chip surface detected by experiments (green square) and computed by 2D (blue dots) and 3D (pink dots) models

Comparison between experimental and numerical results highlights a very good agreement. The best correspondence is obtained for the vertical disposition of the case and, as attended, for the three-dimensional model of the physical system (maximum relative gap with respect to experimental results less than 3.5%).

5. Horizontally arranged DIMM

In this section the main results obtained by the numerical modelling of the memory modules horizontally arranged are presented.

5.1 Transient fluid-dynamics during DIMM heating

Results obtained by approximating the physical system by its transversal section are presented in following. In Figure 14 (A-D) we report thermal and fluid-dynamical fields for 4 time steps of a transient analysis performed in a temporal range of 0.1 [s].

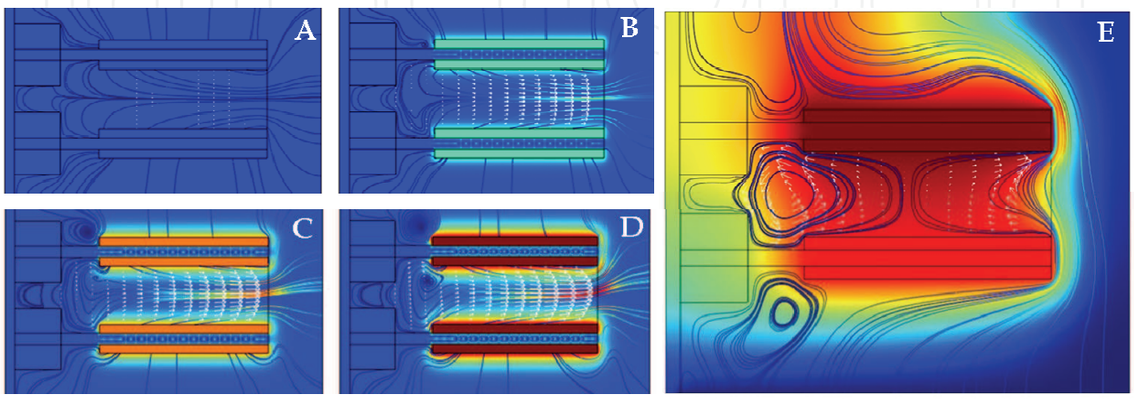

Figure 14. Transient temperature fields, streamlines of flow and velocity vectors for t ∈ {0 (A); 0.03 (B); 0.07 (C); 0.1 (D)} [s] and for achieved stationary conditions

System is initialized with rest conditions for fluid, T_{AMB}=30 [°C] (t=0 [s]) and a power Q_D=1 [W] globally supplied to the heat sources. The motion transient time for the system has been detected to be very short. Fluid, semi-confined by the overlapped solid layers, is quickly propelled by chips heating and forced to flow outside the semi-confined region (t=0.03 [s]). Velocity field assumes a pseudo-parabolic profile, reaching its maximum in correspondence of the middle region between overlapped boards (t=0.07 [s]). At the same time, a convective fluid structure begins to form close to the upper circuit board and backside socket. Then, this structure assumes a defined shape while a second dissipative re-circulating cell appears in the semi-confined region of fluid (t=0.1 [s]). At steady conditions (Figure 14E) this "internal" re-circulating cell increases, extending over a half about of the semi-confined cavity. Its rotational motion induces arising of a further dissipative "half-roll", standing close to the geometrical end of the solid boards and chips. Generation of counter-rotating convective cells is induced by the onset of thermo-convective instability, certainly amplified both by adherence conditions at boundaries and geometrical singularity in the cavity shape. Externally, the flow pattern is worthy influenced by flowing-up air, that sensibly modify the shape of the convective transient roll observed in the left top portion of the considered domain. On the other hand, in the left bottom volume of air, a dissipative flow structure is clearly observable. Temperature field is strongly dependent on fluid flow. The maximum detected value of velocity is about 0.095 [m/s]. Chips arranged on the top circuit board are obviously hotter than those placed on the bottom one. Maximum detected temperature is about 54 [°C] for the discussed simulation.

5.2 Transient and steady approach in solving governing equations

The most part of results presented in this study comes from solution of conservation equations in their steady formulation. The choice of solving system in steady condition arises from the idea of considering the technological devises in their thermal most unfavourable operative conditions, that consist in constant electrical load of alimentation equal to the maximum value indicated by technical documentation of their constructors. In order to validate the steady approach for solution, a comparison has been preliminary made between results obtained for 2D approximation both by transient and stationary analysis. Figure 15 shows thermal fields and streamlines of flow, on a transversal section of the memory modules, evaluated by transient (left side) and steady (right side) solution of equations (1), respectively.

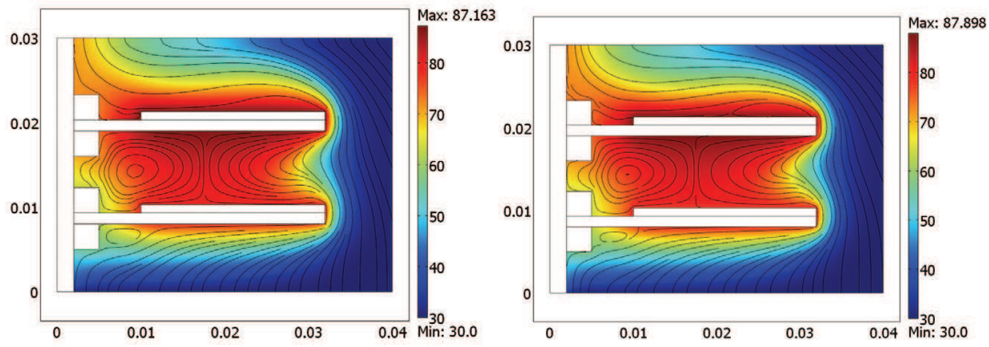

Figure 15. Comparison between transient (left) and steady (right) thermal-dynamical fields

Topology of flow is quite identical for both cases: a primary motion field made of fluid flowing from the bottom boundary of the domain to the upper section turning around the solid domains, and a secondary motion field characterized by the occurrence of a longitudinal convective roll developing in the semi-confined enclosure between the horizontal circuit boards. Drawn thermal levels also show good agreement each other, with a relative discrepancy for the maximum detected temperature of 0.84 %.

5.3 Influence of spacing between thermal sources

Three-dimensional simulations have been carried-out for different models approximating the considered DIMM. At first we studied portions of the electronic device, delimited by transversal surfaces considered as symmetry/slipping plans. Models containing 1 and 2 chips arranged on each top surface of the overlapped PCB were firstly studied. The aim of this investigation consists in studying the influence of spacing between thermal sources. From results it appears that small increasing in chip's spacing highly influences flow pattern of the convective roll detected in the semi-confined region between the overlapped boards. Figure 16 shows comparison between one portion of two overlapped memory modules solved imposing different lateral spacing between thermal sources. It is to notice as the thermo-convective roll does not stand confined in the backside of the semi-confined cavity when spacing is increased. Otherwise, it extends over lateral regions adjacent to the chip, improving convective transfer in dissipating thermal energy.

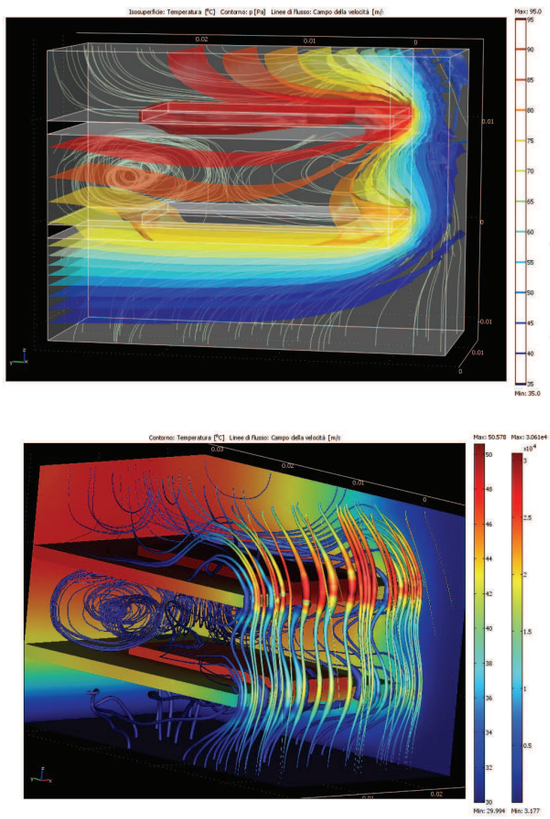

Figure 16. Streamlines of flow and thermal levels for one portion of overlapped memories arranging one chip on top surfaces: influence of chip spacing on convective heat transfer

5.4 Analysis of thermal and fluid-dynamical behaviour during operative conditions

From 3D simulations the motion field of fluid for complete overlapped DIMM appears more complex. As reported in Figure 17, where normalized velocity vectors are plotted in longitudinal and transversal sections, the mean flow exhibits a pronounced chimney effect in correspondence of the central upper chips. The internal flow maintains the longitudinal convective roll flow pattern highlighted by 2D analysis, but developing of thermo-convective instability is seen more articulated. In fact the re-circulation structure is not limited to the backside of the semi-confined cavity, but it also extends around the lateral bounds of the air volume comprised by the overlapped circuit boards. Extension of convective eddy over the lateral portions of volume, close to the lateral guides on the left side, and in correspondence of the half-cross section on the right side, is illustrated in Figure 18. The convective structure assumes a helicoidally developing: fluid particles rotating around the longitudinal roll axis straightly shift along the axis direction. Transport direction mainly follows the way from the lateral guides to the transversal half-cross section of the geometry, where the convective eddy results more intensely developed. From a thermal point of view, the elucidated flow pattern involves the following comments: the maximum value of temperature is detected in correspondence of the third chip standing on

the upper circuit board, as illustrated in Figure 18 where thermal distribution on solid interfaces is plotted.

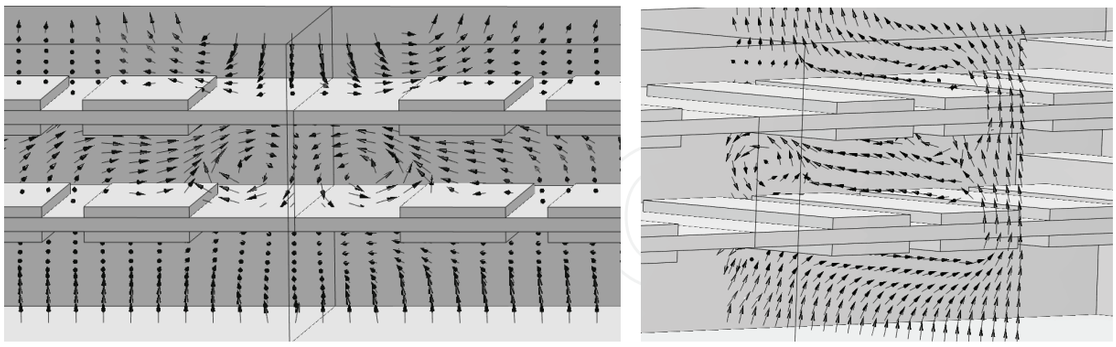

Figure 17. Velocity vectors in longitudinal and transversal sections

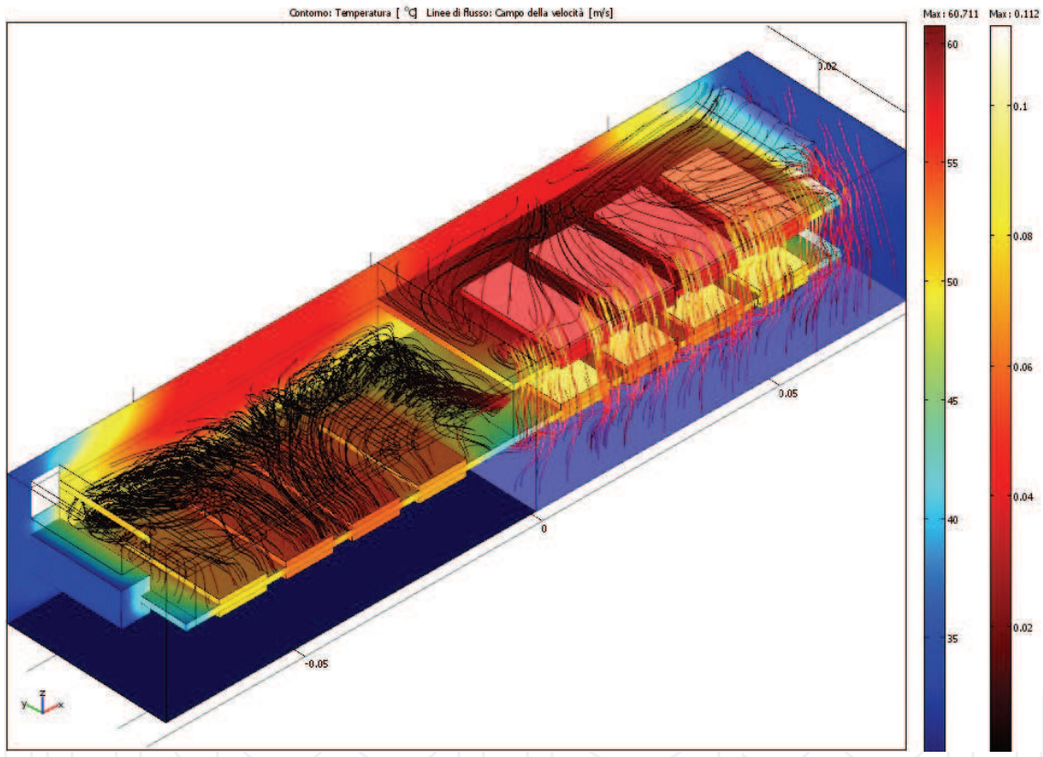

Figure 18. Temperature distribution and streamlines of flow for a double 16-chips model of DIMM obtained for T_{AMB}=30 [°C] and Q_D=0.5 [W] (one PCB is suppressed in plotting)

Convective thermal flux reaches its maximum value close to the right top portion of the fluid volume. As a matter of fact, thermal energy produced inside the semi-confined control volume is worthy dissipated by the discussed dynamical roll, that transports and "ejects" it upward, very close to the middle region of the fluid domain. The illustrated thermal fields well agree with the range of operative temperature indicated by leading DIMM constructors. In fact, in absence of forced airflow, and depending on the benchmark memory stress software applied, a temperature range of 75-95 °C is experimentally measured. Parametric simulations as function of Q_D and T_{AMB} have been carried out for the complete

double DIMM model. From the obtained results a sixth order polynomial fitting law is proposed in order to correlate the maximum detected temperature with the supplied power to the DIMM and the ambient temperature. The proposed correlation equation is reported below:

$$T_{\max} = -19,5 \cdot Q_D^{\,6} + 99,3 \cdot Q_D^{\,5} - 204 \cdot Q_D^{\,4} + 216,9 \cdot Q_D^{\,3} - 132 \cdot Q_D^{\,2} + 93,78 \cdot Q_D + T_{AMB} \quad (5)$$

Simulated maximum temperature values (T_{sim}) are compared with those obtained by applying the above fitting law (T_{fit}) in Table 3.
Reported values for T_{AMB} {30; 35; 40} [°C] are listed as function of Q_D (0.1; 1.2 [0.1]) [W]. Relative gaps between simulated and analytically evaluated temperature are also reported in Table 3. As readable, the maximum gap for the studied Q_D range of variation is 0.61 %.

Q_D	T_{AMB} = 40 [°C]			T_{AMB} = 35 [°C]			T_{AMB} = 30 [°C]		
[W]	T_{sim} [°C]	T_{fit} [°C]	gap %	T_{sim} [°C]	T_{fit} [°C]	gap %	T_{sim} [°C]	T_{fit} [°C]	gap %
0.1	48.45	48.25	0.40	43.43	43.25	0.40	38.41	38.25	0.41
0.2	54.94	54.91	0.06	49.89	49.91	0.03	44.84	44.91	0.15
0.3	60.77	60.67	0.16	55.69	55.67	0.03	50.60	50.67	0.15
0.4	66.19	65.96	0.35	61.07	60.96	0.18	55.94	55.96	0.04
0.5	71.33	71.01	0.45	66.17	66.01	0.24	61.00	61.01	0.01
0.6	76.24	75.89	0.46	71.04	70.89	0.21	65.84	65.89	0.09
0.7	80.98	80.65	0.41	75.75	75.65	0.13	70.50	70.65	0.21
0.8	85.58	85.27	0.36	80.31	80.27	0.05	75.02	75.27	0.33
0.9	90.05	89.74	0.35	84.74	84.74	0.01	79.42	79.74	0.40
1.0	94.42	94.05	0.39	89.07	89.05	0.02	83.71	84.05	0.40
1.1	98.70	98.22	0.48	93.31	93.22	0.09	87.91	88.22	0.35
1.2	102.89	102.26	0.61	97.46	97.26	0.21	92.04	92.26	0.24

Table 3. Simulated and analytical maximum temperature values on DIMM and their relative gaps as function of ambient temperature and thermal load

5.5 Simplifying hypotheses in model implementation

As known, 3D numerical models involve in very expensive computations, both for hardware and time needed for obtaining reliable results. Therefore, the goal of this study also was spending attention in analyzing hypotheses able to simplify the numerical model, maintaining the same standard of result reliability with respect to accuracy assured by more detailed schemes. Simplification of physical system allows to drastically reduce degrees of freedom of the numerical model, so that memory space and computational time can be saved. The first tested hypothesis concerning simplification of the numerical model consists in outlining complete DIMM by one transversal half portion only. In Figure 19 thermal distribution and streamlines of flow for a model are plotted. It represents a half of a twin DIMM of 8 top-arranged chips.
Lateral guides supporting PCB are observable in the left part of the simulated geometry, as well as the socket in its backside. The right transversal section surface represents the considered symmetry/slipping section of the system. Thermal and dynamical fields presented in Figure 19 are obtained for a supplied power Q_D=1 [W] and for T_{AMB}=30 [°C]. Results carried-out by exploiting symmetry conditions seem to be consistent: the range of

the simulated operative temperatures, and the maximum detected value (T ≈ 86 [°C]), well fit with those suggested by the leading constructors of this kind of devices. The second simplifying adopted strategy consists in retaining that the sub-domain simulating the sockets (in the backside of the system) could be suppressed without causing sensible variation in temperature distribution and velocity fields. Following this idea, a simplified model, see Figure 20, giving, for the same level of mesh refinement, a lower number of d.o.f. has been tested in order to replace the above discussed one. In Table 4 a brief comparison between socket and no-socket model is proposed by reporting maximum values of velocity, temperature, Reynolds number and Rayleigh number obtained for both representations. From a global point of view, thermal behaviour of system seems to be not very affected by model simplification, while dynamics appears more sensitive. Suppression in fluid domain of the small sized enclosure due by sockets representation does not modify internal thermo-convective flow pattern. In fact, the secondary flow, assuring heat evacuation in the semi-confined region of the system, does not show any relevant modification with respect to the complete model.

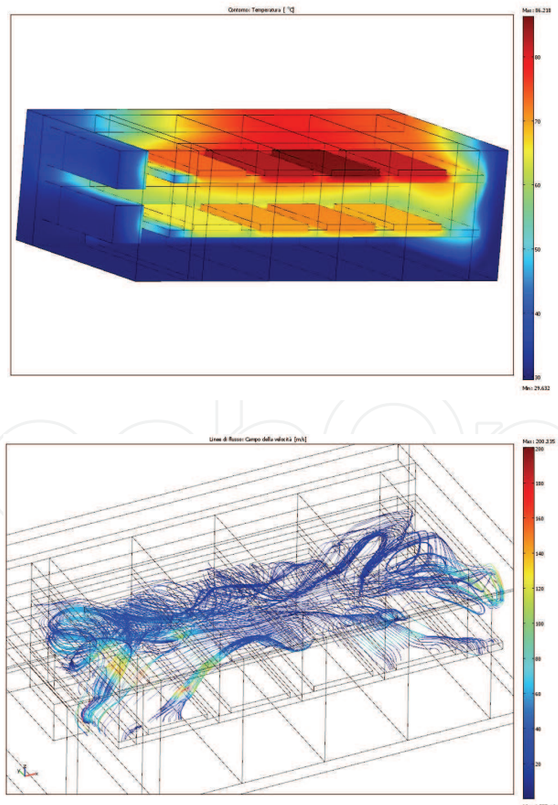

Figure 19. Thermal distribution and streamlines of flow for 8-chip overlapped memories represented by one symmetrical half of their geometry

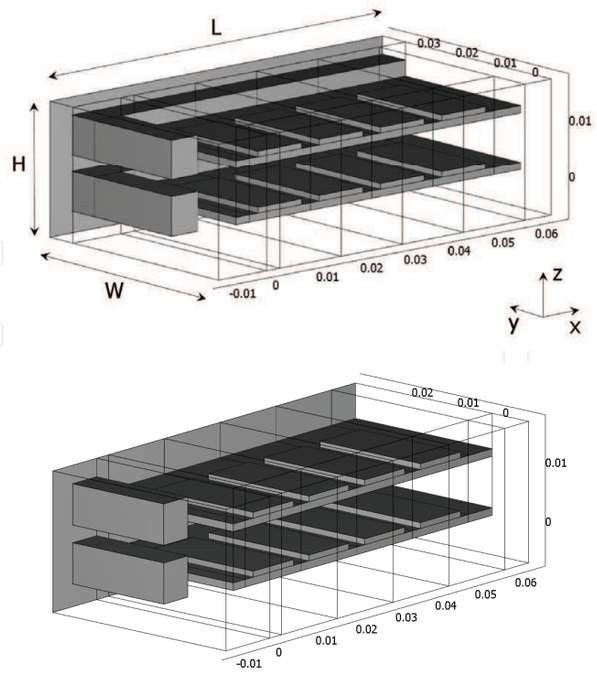

Figure 20. Geometrical model of twin overlapped 8-chip memories outlined with (left side) and without (right side) socket in their backside

	Socket	No-Socket	Relative gap (%)
U_{max}	0.142	0.154	8.31
T_{max}	87.7	87.9	0.18
Re_{max}	423	455	7.41
Ra_{max}	2205	2210	0.22

Table 4. Comparison between socket and no-socket models

6. Vertically arranged DIMM

Some results concerning memory modules vertically arranged have been yet discussed in the section related to the numerical models validation. From Figure 21 it can be deduced as fluid-dynamical fields for vertical disposition result less complex than those highlighted for the horizontal configuration. Fluid is propelled by buoyancy force to flow up without encountering obstacles in its path. Heat is vertically transported and for that reason the integrated circuits arranged in the top portion of the modules manifest higher thermal levels. From results analysis it globally appears that vertical disposition is preferable from a thermal point of view with respect to the horizontal one. For a fixed value of imposed thermal load, the vertical configuration assures lower thermal levels on the package. However, the interest in studying this configuration was motivated to investigate on convective heat transfer not only in natural convection condition, but also in mixed convection condition. Models considering imposed air flow rate coming from the bottom surface of the outlined air volume have been built and convective heat transfer coefficient

have been computed for several values of fixed velocity for air. The non-dimensional parameter chosen in order to quantify the convective heat transfer rate is the local Nusselt number evaluated on chip top surfaces, defined as:

$$Nu = \frac{\frac{1}{H_C \cdot L_C}\int_{z_1}^{z_2}\int_{y_1}^{y_2}\frac{\partial T}{\partial x}dydz}{(T_C - T_{AMB})/L}$$

The range of fixed values for velocity inlet flow (0.1÷0.2 [m/s]) has been limited to maximum velocity values characteristics of fluid-dynamical motion fields observed in natural convection condition. This procedure allows to reproduce physical systems where natural and forced convection effects in heat transfer could be considered comparable. In Table 5 natural and mixed convection configuration are compared from a thermal point of view. The relative gap, concerning the main temperature evaluated on each chip surface of one memory module (IC 1-16, see Fig. 9) and the computed local Nusselt number, between natural and mixed convection conditions are listed. Relative gaps are evaluated both for minimum (v=0.1 [m/s]) and maximum (v=0.2 [m/s]) velocity values chosen for the inlet forced flow. From analysis of results it appears that benefit of forced flow mainly concerns IC arranged at the bottom position and on external surfaces of the PCB. It is to notice as decreasing in thermal levels on IC surfaces is comprised in the thin range 1-6%, while increasing in heat transfer coefficient results very fluctuant and, depending on IC position, achieves values up to 300%. This item can be explained: the IC standing on the top positions are in natural convection subject to air flow at the higher velocity, while IC standing on the bottom position are plunged in fluid almost at rest conditions. In mixed convection configuration air flow is quantitatively distributed homogeneously, so that the best advantage in heat transfer coefficient is related to those IC arranged in the most unfavourable position when any forced flow is imposed.

7. Conclusion

This chapter highlights the opportunity to exploit a numerical approach in order to simulate thermal and fluid-dynamical behaviour of electronic devices. The goal mainly consists in disposing of a predictive and flexible tool for characterising those equipments during several functioning conditions avoiding expensive experimentations. On the other hand, the chapter also underlines the unquestionable importance of a validation step for the numerical model, strictly needed in order to assure effectiveness and reliability of the results carried-out. As applications of the proposed approach, Dual Inline Memory Module dissipation is studied both for horizontal and vertical arrangement and for natural and mixed convection heat transfer mechanism. Detected temperature values are globally in accordance with data reported in technical sheets of the leading constructors of the studied technological devices. Numerical results are mainly carried-out as function of operational parameters, such as ambient temperature and power supplied to the memory modules. Several models are presented, that also resume the adopted strategy in order to optimise them, testing simplifying hypotheses as: opportunity of considering geometrical symmetries, possibility of suppressing in models structural elements not significantly modifying thermal and fluid-dynamical behaviour of the system, reliability of 2D results

with respect to 3D ones. The onset of a thermo-convective instability is highlighted in horizontal configuration. It manifests in arising of complex three-dimensional flow patterns, principally consisting in a dissipative roll that helicoidally develops close to the lateral and backside boundaries of the considered fluid domain. That convective structure seems to significantly contribute in heat dissipation of system, transporting and ejecting thermal energy in correspondence of the frontal opened section of the semi-confined geometry. Concerning thermal efficiency, the vertical configuration is found to be preferable with respect to the horizontal one. Instead, from a theoretical point of view the horizontal disposition results much more interesting to be studied. Non-dimensional parameters, such as Rayleigh, Reynolds and local Nusselt number, are computed in order to quantify the flow regime and the heat transfer coefficients. In order to produce exploitable results of applied interest, a polynomial fitting law, correlating the maximum detectable temperature for the system with the ambient temperature and the supplied thermal load, is proposed.

IC	$\frac{T_{nat}-T_{v=0.1}}{T_{nat}}\%$	$\frac{T_{nat}-T_{v=0.2}}{T_{nat}}\%$	$\frac{Nu_{v=0.1}-Nu_{nat}}{Nu_{nat}}\%$	$\frac{Nu_{v=0.2}-Nu_{nat}}{Nu_{nat}}\%$
1	1.59	3.25	12.52	32.32
2	1.68	3.34	13.52	35.54
3	1.75	3.59	15.59	39.81
4	1.83	3.89	20.48	48.80
5	2.53	5.27	25.79	47.04
6	3.20	5.81	26.76	47.38
7	3.89	5.86	30.20	54.42
8	4.02	5.30	50.81	85.19
9	1.58	3.23	17.42	34.74
10	1.67	3.38	26.84	53.77
11	1.73	3.56	34.96	70.68
12	1.81	3.86	45.88	115.72
13	2.52	5.24	80.97	228.95
14	3.24	5.93	101.31	291.41
15	3.99	6.06	192.06	311.35
16	4.11	5.46	197.02	327.19

Table 5. Relative gaps in temperature and local Nusselt number between natural and mixed convection conditions

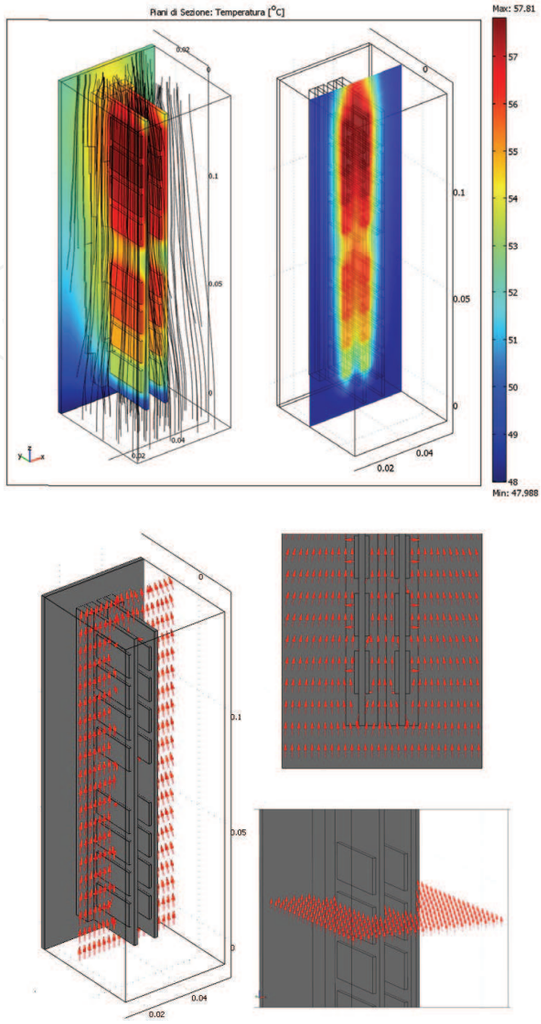

Figure 21. Thermal distribution at fluid-solid interfaces, streamlines of flow and temperature field on a longitudinal section (left side). Velocity vectors in longitudinal and transversal sections of the air volume surrounding the electronic devices (right side)

8. Nomenclature

C_p	isobaric specific heat	[J/(kg K)]
D_h	hydraulic diameter	[m]
g	gravity acceleration	[m/s^2]
H	height of air volume	[m]
h	distance between circuit boards	[m]
k	thermal conductivity	[W/(m K)]
L	length of air volume	[m]
M	molecular mass of air	[kg/mole]

Nu	Nusselt number, $Nu = \frac{1}{H_C \cdot L_C} \int_{z_1}^{z_2} \int_{y_1}^{y_2} \frac{\partial T}{\partial x} dydz \Big/ (T_C - T_{AMB}) \Big/ L$	
n	number of integrated circuits	
p	pressure	[Pa]
Q	thermal flux	[W]
q	specific thermal flux	[W/m^3]
R	Gas constant	[J/(kg mole)]
Ra	Rayleigh number, $gh^3 \Delta\rho / \eta\alpha$	
Re	Reynolds number, $\rho U D_h / \eta$	
T	temperature	[K]
t	time	[s]
$\vec{U}$	velocity vector, $(u, v, w)^t$	
U	norm of velocity, $(u^2 + v^2 + w^2)^{1/2}$	[m/s]
W	width of air volume	[m]

Greek symbols

α	thermal diffusivity	[m^2/s]
η	dynamic viscosity	[Pa s]
ρ	density	[kg/m^3]
Ω	volume	[m^3]

Subscripts

AMB	ambient
C	Chip
D	Dual Inline Memory Modules
P	Printed Circuit Board

9. References

Bae, H.J.; Hyun & J.M. (2004). Time-dependent buoyant convection in an enclosure with discrete heat sources. *International Journal of Thermal Sciences*, Vol. 43, page numbers (3-11), ISSN 1290-0729

Bailey, C.; Lu H. & Wheeler D. (2002). Computational modeling techniques for reliability of electronic components on printed circuit boards. *Applied Numerical Mathematics*, Vol. 40, page numbers (101-117), ISSN 0168-9274

Bhowmik, H. & Tou, K.W. (2005). Experimental study of transient natural convection heat transfer from simulated electronic chips. *Experimental Thermal and Fluid Science*, Vol. 29, page numbers (485-492), ISSN 0894-1777

Brenan, K.E.; Campbell, S.L. & Petzold, L.R. (1989). *Numerical Solution of Initial-Value Problems in Differential-Algebraic Equations*, Elsevier, ISBN 0898713536, New York

da Silva, A.K.; Lorenzini, G. & Bejan A. (2005). Distribution of heat sources in vertical open channels with natural convection, *International Journal of Heat and Mass Transfer*, Vol. 48, page numbers (1462-1469), ISSN 0017-9310

Deuflhard, P. (1974). A modified Newton method for the solution of ill-conditioned systems of nonlinear equations with application to multiple shooting, *Numerical Mathematics*, Vol. 22, page numbers (289-315), ISSN 0168-9274

Dogan, G.; Sivrioglu, M. & Baskaya, S. (2006). Investigation of mixed convection heat transfer in a horizontal channel with discrete heat sources at the top and at the bottom, *International Journal of Heat and Mass Transfer*, Vol. 49, page numbers (2652-2662), ISSN 0017-9310

El Alami, M.; Najam, M.; Semma, E.; Oubarra, A. & Penot, F. (2005). Electronic components cooling by natural convection in horizontal channel with slots, *Energy Conversion and Management*, Vol. 46, page numbers (2762-2772), ISSN 0196-8904

Hanreich, G.; Nicolics, J. & Musiejovsky, L. (2000). High resolution thermal simulation of electronic components, *Microelectronics Reliability*, Vol. 40, pp. 2069-2076,

Harvest, J.; Fleischer, A.S. & Weinstein R.D. (2007) Modeling of thermal effects of heat generating devices in close proximity on vertically oriented printed circuit boards for thermal management applications, *International Journal of Thermal Sciences*, Vol. 46, page numbers (253-261), ISSN 0226-2714

Ortega, A. (1996) Conjugate heat transfer in forced air cooling, In: *Air cooling technology for electronic equipment*, Sung-Jin Kim & Sang-woo Lee, pp. 103-172, CRC Press, ISBN 0849394473

Petrone, G.; Chénier, E. & Lauriat, G. (2004). Stability of free convection in air-filled horizontal annuli: influence of the radius ratio, *International Journal of Heat and Mass Transfer*, Vol. 47, page numbers (3889-3907), ISSN 0017-9310

Petrone, G.; Sorge, G. & Cammarata G. (2007). Thermal dissipation of DIMM in Tower-BTX configuration, *International Journal of Multiphysics*, Vol. 1, page numbers (231-244), ISSN 1750-9548

Towashiraporn, P.; Subbarayan, G.; McIlvanie, B.; Hunter, B.C.; Love, D. & Sullivan B. (2004). The effect of model building on the accuracy of fatigue life predictions in electronic packages, *Microelectronics Reliability*, Vol. 44, pp. 115-127

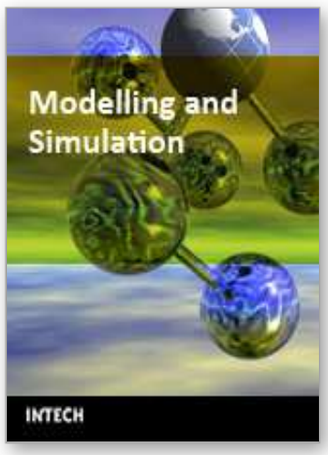

Modelling and Simulation

Edited by Giuseppe Petrone and Giuliano Cammarata

ISBN 978-3-902613-25-7
Hard cover, 688 pages
Publisher I-Tech Education and Publishing
Published online 01, June, 2008
Published in print edition June, 2008

This book collects original and innovative research studies concerning modeling and simulation of physical systems in a very wide range of applications, encompassing micro-electro-mechanical systems, measurement instrumentations, catalytic reactors, biomechanical applications, biological and chemical sensors, magnetosensitive materials, silicon photonic devices, electronic devices, optical fibers, electro-microfluidic systems, composite materials, fuel cells, indoor air-conditioning systems, active magnetic levitation systems and more. Some of the most recent numerical techniques, as well as some of the software among the most accurate and sophisticated in treating complex systems, are applied in order to exhaustively contribute in knowledge advances.

How to reference

In order to correctly reference this scholarly work, feel free to copy and paste the following:

Giuseppe Petrone and Giuliano Cammarata (2008). Numerical Modelling for Thermal Design of Electronic Equipments, Modelling and Simulation, Giuseppe Petrone and Giuliano Cammarata (Ed.), ISBN: 978-3-902613-25-7, InTech, Available from: http://www.intechopen.com/books/modelling_and_simulation/numerical_modelling_for_thermal_design_of_electronic_equipments

INTECH
open science | open minds

InTech Europe
University Campus STeP Ri
Slavka Krautzeka 83/A
51000 Rijeka, Croatia
Phone: +385 (51) 770 447
Fax: +385 (51) 686 166
www.intechopen.com

InTech China
Unit 405, Office Block, Hotel Equatorial Shanghai
No.65, Yan An Road (West), Shanghai, 200040, China
中国上海市延安西路65号上海国际贵都大饭店办公楼405单元
Phone: +86-21-62489820
Fax: +86-21-62489821

IntechOpen